J. Webster (ed.), *Wiley Encyclopedia of Electrical and Electronics Engineering*

HORN ANTENNAS

A horn antenna is a length of conducting tube that is flared at one end and used for the transmission and reception of electromagnetic waves. For an efficient transition between guided and radiated waves the horn dimensions must be comparable to the wavelength. Consequently, horns are used mostly at centimeter and millimeter wavelengths. At lower or higher frequencies they are inconveniently large or small, respectively. They are most popular at microwave frequencies (3 GHz to 30 GHz) and higher frequencies (30 GHz to 300 GHz), as antennas of moderate directivity or as feeds for reflectors or elements of arrays.

Since acoustic horns have been in use since prehistoric times, the design of horns as musical instruments was a highly developed art well before the appearance of the first electromagnetic horns. This occurred shortly after Hertz first demonstrated the existence of electromagnetic waves in 1888. Experimenters placed their spark gap sources in hollow copper tubes [Figs. 1(a) and 5(a)]. These tubes acted as high-pass filters for microwave and millimeter-wave radiation from the open end. In London in 1897, Chunder Bose used rectangular conducting tubes with "collecting funnels," or pyramidal horns [Fig. 1(d)], in his demonstrations at 5 mm and 25 mm wavelengths [see Ramsay (1)]. Thus the electromagnetic horn antenna was introduced, but this early beginning of microwave invention closed with Marconi's demonstration that longer wavelengths could be received at greater distances. Horns were too large to be practical at those wavelengths, and it was almost 40 years before microwave horns reappeared with the need for directive antennas for communications and radar. Horns alone were often not sufficiently directive; but combined in an array or with a lens [Fig. 4(a)], or more often a parabolic reflector [Figs. 4(b) and 4(c)], highly directive antenna beams are obtained.

Radiating Waveguides and Horns

Horns are normally fed by waveguides supporting only the dominant waveguide mode. For a rectangular waveguide [Fig. 1(a)] with TE_{01} mode propagation only, these dimensions in wavelengths λ are $\lambda/2 < a < \lambda$ and $b \approx a/2$. Open-ended waveguides have broad radiation patterns, so when they are used as a feed for a reflector, there is substantial spillover, or radiation missing the reflector and radiation directly backwards from the feed. To increase the directivity of a radiating waveguide and its efficiency as a reflector feed, for example, its aperture dimensions must be enlarged, because the beamwidth of an aperture of width $a \gg \lambda$ is proportional to λ/a radians.

This waveguide enlargement by a flare characterizes horns. The aperture fields of a horn are spherical waves originating at the horn apex (Fig. 2). The path from the horn apex to the aperture plane at a distance x from the aperture center of a horn of slant length ℓ is

$$\rho = ((\ell \cos \alpha)^2 + x^2)^{1/2} \approx \ell \cos \alpha + \frac{x^2}{2\ell \cos \alpha} \qquad (1)$$

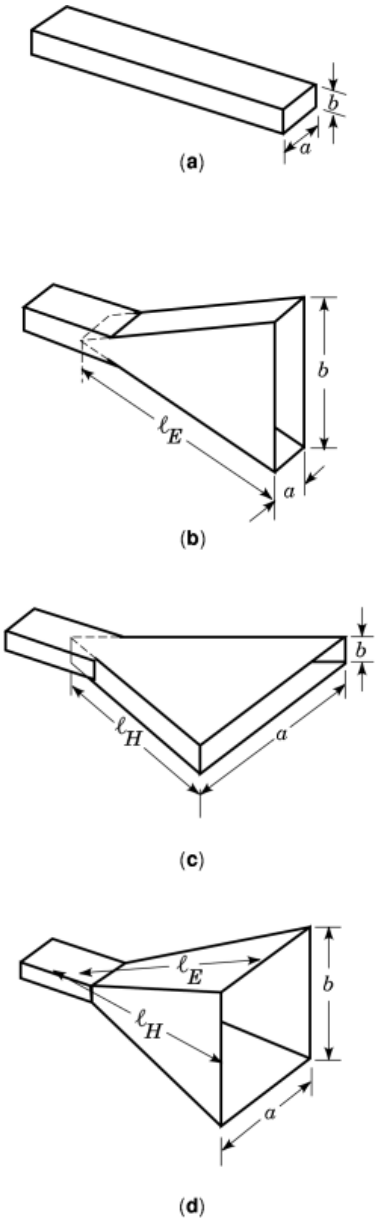

Fig. 1. (a) Open-ended rectangular waveguide. (b) E-plane sectoral horn. (c) H-plane sectoral horn. (d) Pyramidal horn.

when $x \ll \ell \cos \alpha$. Thus the phase variation in radians across the aperture for small flare angles α is approximately $kx^2/(2\ell)$, where $k = 2\pi/\lambda$ is the propagation constant. This quadratic phase variation increases with increasing flare angle, thus reducing directivity increase due to the enlarged aperture dimension. It is

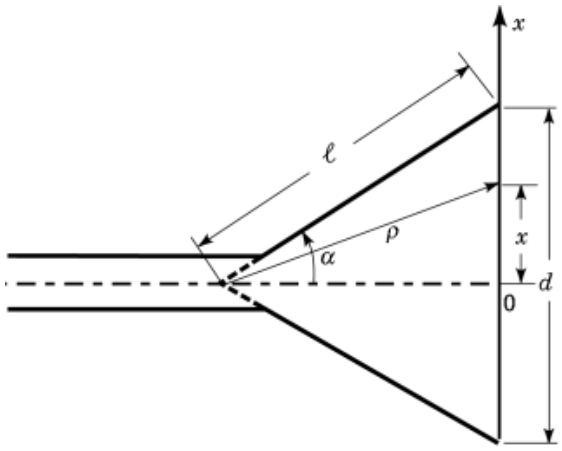

Fig. 2. Effect of horn flare on the aperture field phase of a horn.

convenient to quantify aperture phase variation by the parameter

$$s = \ell(1 - \cos\alpha)/\lambda \approx \frac{d^2}{8\lambda\ell}, \qquad d \ll \ell \tag{2}$$

which is the approximate difference in wavelengths between the distance from the apex to the edge ($x = d/2$) and the center ($x = 0$) of the aperture. The radiation patterns of Figs. 3(a) and 3(b) [from Love (2)] show the effect of increasing s on the E- and H-plane radiation patterns of sectoral and pyramidal horns. The main beam is broadened, the pattern nulls are filled, and the sidelobe levels raised over those for an in-phase aperture field ($s = 0$). With large flare angles, radiation from the extremities of the aperture can be so out of phase with that from the center that the horn directivity decreases with increasing aperture width.

The adverse effects of the flare can be compensated by a lens in the aperture [Fig. 4(a)]; but because that adds to the weight and cost and because bandwidth limitations are introduced by matching the lens surfaces to reduce reflections, it is not usually done except in some millimeter wave applications. Instead a combination of aperture width and flare length in wavelengths is chosen which provides maximum axial directivity or minimum beamwidth. This is an "optimum" horn design. To achieve higher directivity or narrower beamwidth for a given aperture width, a longer horn is required.

Sectoral horns [Figs. 1(b) and (c)] are rectangular waveguides flared in one dimension only. The incident waveguide mode becomes a radial cylindrical mode in the flared region of the horn. Since radiation pattern beamwidths are inversely proportional to aperture dimensions in wavelengths, sectoral horns have beams which are narrow in the plane containing the broad dimension. Such fan-shaped beams may be useful for illuminating elongated parabolic reflectors or parabolic cylinder reflectors.

A pyramidal horn [Fig. 1(d)] is flared in both waveguide dimensions and thus is more adaptable both as a reflector feed and on its own. The forward radiation pattern may be calculated quite accurately from Kirchhoff diffraction theory for all but small horns. The TE_{01} rectangular waveguide mode yields an aperture field uniform in one dimension (in the E plane) and cosinusoidal in the other (the H plane). A comparison of Figs. 3(a) and 3(b) shows that this results in higher sidelobes in the E plane and, for a square aperture, a narrower beam. Pyramidal horns are relatively easily constructed, and for all but small horns their axial gain can be predicted accurately. Consequently they are used as gain standards at microwave frequencies; that is,

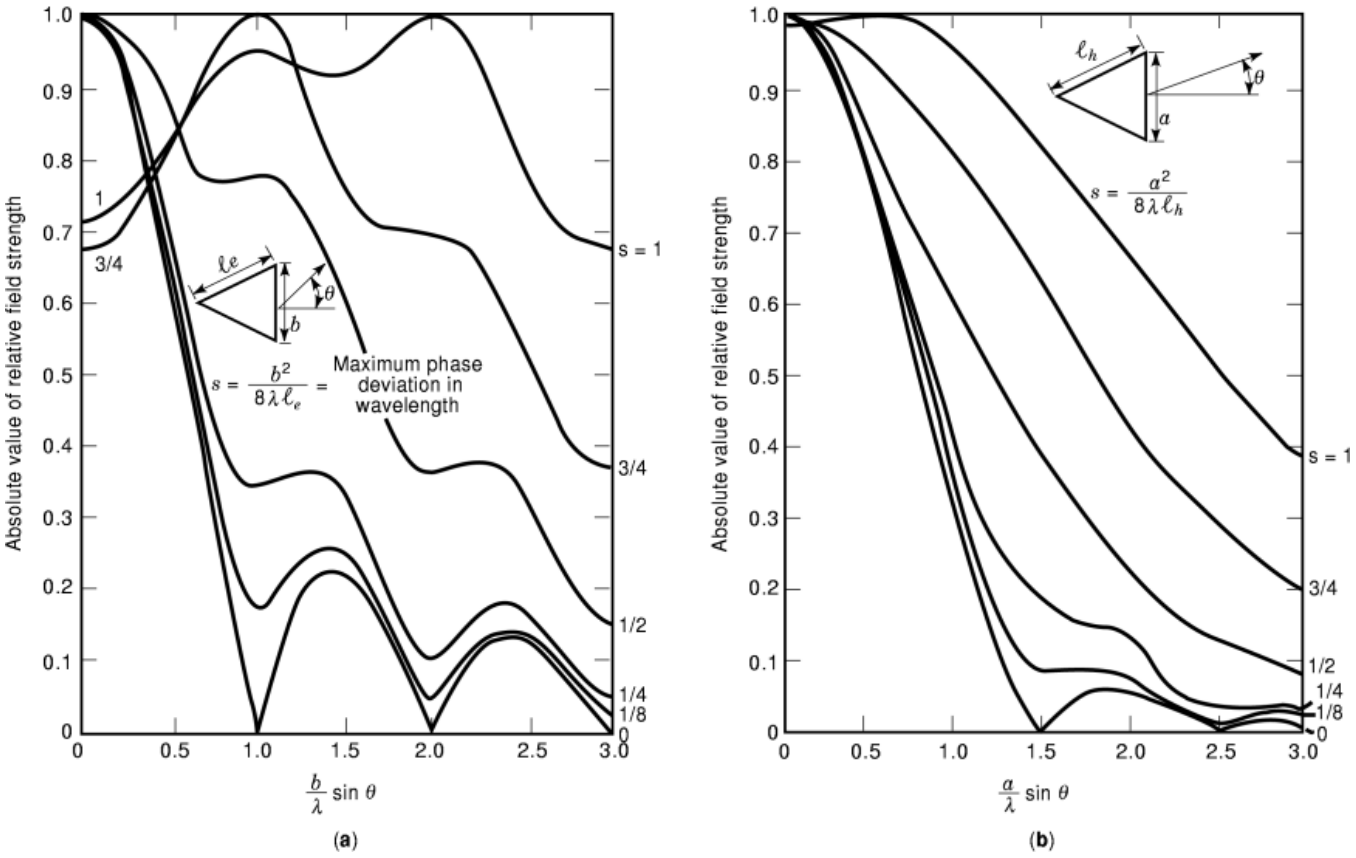

Fig. 3. Universal radiation patterns of sectoral and pyramidal horns flared in the (a) E plane and (b) H plane. The parameter s equals $b^2/8\lambda\ell_E$ in (a) and $a^2/8\lambda\ell_H$ in (b), and $2\pi s/\lambda$ is the maximum phase difference between the fields at the center and the edge of the aperture [© 1984 McGraw-Hill, Inc., from Love (2)].

they are used to experimentally establish the gain of other microwave antennas by comparing their response with the same illuminating field.

Most of the preceding remarks on open-ended rectangular waveguides and pyramidal horns apply also to open-ended circular waveguides and conical horns [Figs. 5(a) and (b)]. For propagation of the lowest-order mode (TE_{11}), only in a circular waveguide the interior diameter must be $0.59\lambda < a < 0.77\lambda$. This mode has a uniform aperture field in the E plane and an approximately cosinusoidal distribution in the orthogonal H plane. This appears, modified by a quadratic phase variation introduced by the flare, in the aperture field of the horn. Consequently the E-plane radiation pattern of the horn is narrower, but with higher sidelobes than the H-plane pattern and the radiated beam is elliptical in cross section. In addition, cross-polarized fields appear in pattern lobes outside the principal planes.

Horn Feeds for Reflectors

Many refinements to horns arise from their use as efficient feeds for parabolic reflectors, particularly in satellite and space communications and radio astronomy. The phase center, where a horn's far radiation field appears

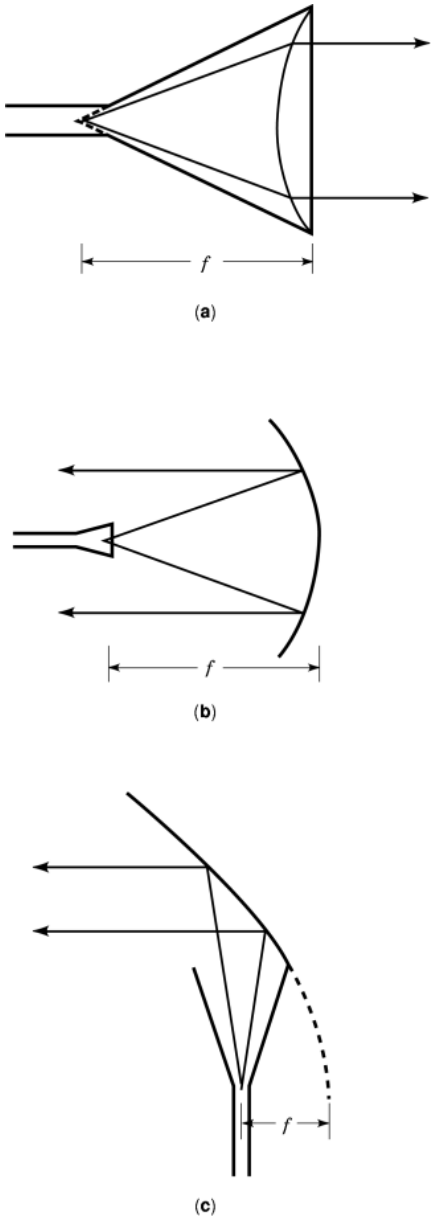

Fig. 4. (a) Horn aperture field phase correction by a lens. (b) Parabolic reflector fed by a horn. (c) Horn reflector antenna. f is the focal length of the lens or reflector.

to originate, must be placed at the focus of the reflector [Fig. 4(b)]. This phase center is within the horn on the horn axis and depends on the flare angle and aperture distribution. For both rectangular and conical horns the position of the phase center is not the same in the E and H planes, or planes containing the electric and magnetic field vectors, respectively. A phase center can be calculated from the average of the positions of the

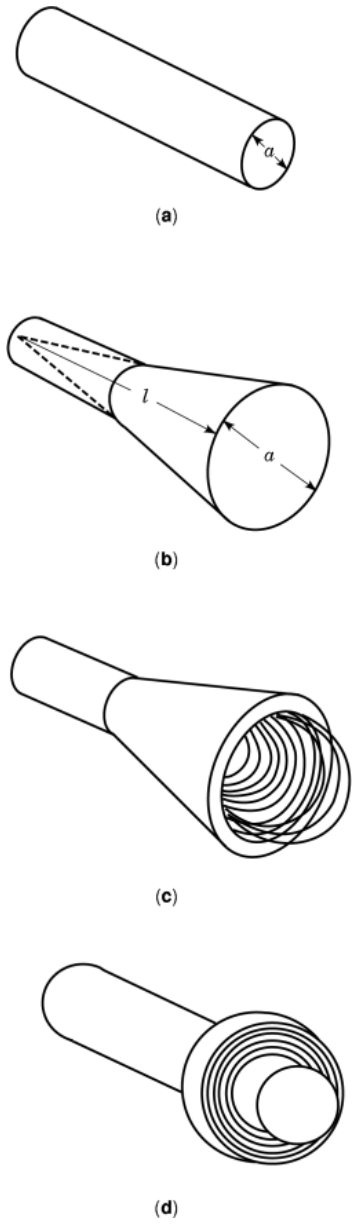

Fig. 5. (a) Open-ended circular waveguide. (b) Conical horn. (c) Corrugated horn. (d) Circular waveguide with corrugated flange.

E- and *H*-plane phase centers, or it can be determined from the position of the feed which maximizes the gain of the reflector antenna.

For efficient reflector aperture illumination the feed horn radiation pattern should approximately match the shape of the reflector's aperture, and illuminate it essentially uniformly and with minimal spillover, or radiation missing the reflector. Pyramidal horns may seem suitable for rectangular apertures because their

beams are rectangular in cross section, and conical horns may seem a natural choice for a circular aperture; but efficient aperture illumination is not obtained in either case, because their principal plane patterns differ. Both horns have high E-plane pattern sidelobes and low H-plane sidelobes. A dual (TE_{11}/TM_{11}) mode conical horn provides equal E- and H-plane beamwidths and equally low sidelobes and is an efficient feed for a circular aperture over a narrow frequency band [Love (3), p. 195]. (Reference 3 contains reprints of most earlier significant articles on horn antennas.) A broadband solution achieves an axisymmetric beam with annular corrugations on the interior surfaces of a conical horn [Fig. 5(c)] [Love (3), pp. 248, 277]. These produce a horn aperture field distribution which is approximately cosinusoidal across the conical horn aperture in all directions and hence an axisymmetric radiation pattern with low sidelobes. Such corrugations in the E-plane interior walls only of a pyramidal horn will produce a nearly cosinusoidal E-plane aperture distribution, and consequently similar E-plane and H-plane radiation patterns for a square horn aperture.

A feed for a small circular aperture reflector which is more easily constructed than a corrugated conical horn, but with a less axisymmetric radiation pattern, is an open-ended circular waveguide ringed by a recessed disc of approximately quarter-wavelength-deep corrugations [Fig. 5(d)]. These corrugations suppress back radiation from the feed and thus improve the aperture illumination over that of a simple open circular waveguide [Love (3), pp. 181, 226]. Combined with dual mode excitation, this arrangement provides an efficient field for a paraboloidal reflector.

Radiation from Apertures

The far-field radiation pattern of an aperture can be calculated exactly from the Fourier transform of the tangential fields in the entire aperture plane. Either electric or magnetic aperture fields may be used, but for apertures in space a combination of the two gives the best results from the usual assumption that aperture plane fields are confined to the aperture and negligible outside it. This aperture field is assumed to be the undisturbed incident field from the waveguide. For apertures with dimensions larger than several wavelengths, a further simplifying assumption usually made is that the aperture electric and magnetic fields are related as in free space.

Rectangular Apertures. With the above assumptions, at a distance much larger than the aperture dimensions, the radiated electric field intensity of a linearly polarized aperture field $E_x(x, y, 0)$ in the coordinates of Fig. 6(a) is

$$\boldsymbol{E}(r, \theta, \phi) = \boldsymbol{A}(r, \theta, \phi) \int_{-b/2}^{b/2} \int_{-a/2}^{a/2} E_x(x, y, 0) e^{j(k_1 x + k_2 y)} \, dx \, dy \quad (3)$$

Here

$$\begin{aligned} k_1 &= k \sin\theta \cos\phi \\ k_2 &= k \sin\theta \sin\phi \end{aligned} \quad (4)$$

and

$$\boldsymbol{A}(r, \theta, \phi) = j \frac{e^{-jkr}}{2\lambda r} (1 + \cos\theta)(\hat{\theta} \cos\phi - \hat{\phi} \sin\phi) \quad (5)$$

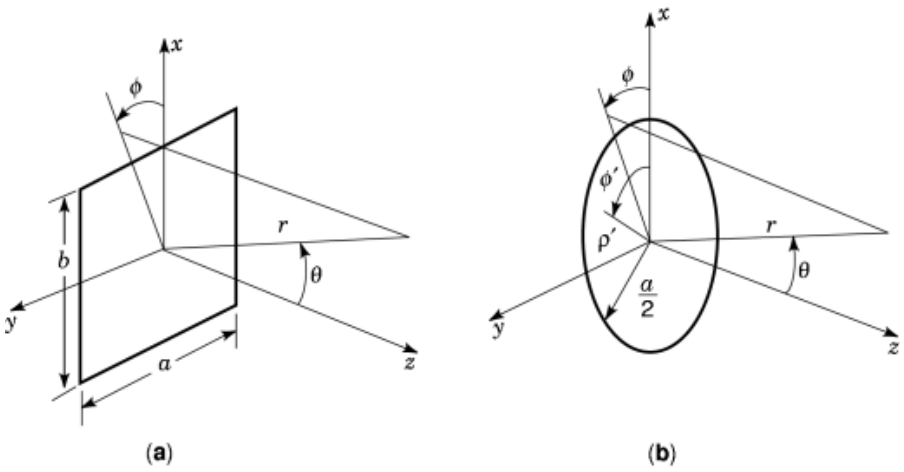

Fig. 6. Coordinates for radiation from (a) rectangular and (b) circular apertures.

is a vector defining the angular behavior of the radiation polarization for an aperture in space. For an aperture in a conducting plane, it is more accurate to use

$$\boldsymbol{A}(r,\theta,\phi) = j\frac{e^{-jkr}}{\lambda r}(\hat{\theta}\cos\phi - \hat{\phi}\sin\phi\cos\theta) \tag{6}$$

which, since it is based on the aperture plane electric fields only, fully satisfies the assumption of a vanishing tangential field in the aperture plane outside the aperture. Consequently, radiation fields of open-ended waveguides and small horns can be calculated accurately from Eq. (3) with Eq. (6) if they are mounted in a conducting plane. Clearly, Eqs. (5) and (6) differ significantly only for large angles θ off the beam axis.

If the aperture field is separable in the aperture coordinates—that is, in Eq. (3), $E_x(x, y, 0) = E_0E_1(x)E_2(y)$, where $E_1(x)$ and $E_2(y)$ are field distributions normalized to E_0—then the double integral is the product of two single integrals:

$$\boldsymbol{E}(r,\theta,\phi) = \boldsymbol{A}(r,\theta,\phi)E_0F_1(k_1)F_2(k_2) \tag{7}$$

where

$$F_1(k_2) = \int_{-a/2}^{a/2} E_1(x)e^{jk_1y}\,dx \tag{8}$$

$$F_2(k_2) = \int_{-b/2}^{b/2} E_2(y)e^{jk_2y}\,dy \tag{9}$$

define the radiation field.

Open-Ended Waveguides

Rectangular Waveguides. With the TE_{01} waveguide mode the aperture field

$$E_x(x, y, 0) = E_0 \cos \frac{\pi y}{a} \tag{10}$$

in Eq. (7) yields the following for Eqs. (8) and (9):

$$F_1(k_1) = b \frac{\sin\left(\frac{k_1 b}{2}\right)}{\frac{k_1 b}{2}} \tag{11}$$

$$F_2(k_2) = a \left(\frac{\cos\left(\frac{k_2 a}{2}\right)}{\pi^2 - (k_2 a)^2} \right) \tag{12}$$

This defines the radiation pattern in the forward hemisphere $-\pi/2 < \theta < \pi/2$, $0 < \phi < 2\pi$. If the aperture is in space, then Eq. (5) is used for $\boldsymbol{A}(r, \theta, \phi)$, but this is not an accurate solution since the aperture dimensions are not large. Rectangular waveguides mounted in conducting planes use Eq. (6) for $\boldsymbol{A}(r, \theta, \phi)$ in Eq. (7), which then accurately provides the far field. The pattern has a single broad lobe with no sidelobes. For large apertures, plots of the normalized E-plane ($\phi = 0$) and H-plane ($\phi = \pi/2$) patterns of Eq. (7) appear in Figs. 3(a) and 3(b) for those of a horn with no flare ($s = 0$), but without the factor $(1 + \cos \theta)/2$ from Eq. (5) or $\cos \theta$ from Eq. (6).

Circular Waveguides. The dominant TE_{11} mode field in circular waveguide produces an aperture field distribution which in the aperture coordinates ρ', ϕ' of Fig. 6(b) is

$$\boldsymbol{E}(\rho', \phi') = E_0 \left[\hat{\rho}' \frac{J_1(k_c \rho')}{k_c \rho'} \cos \phi' + \hat{\phi}' J_1'(k_c \rho') \sin \phi' \right] \tag{13}$$

where J_1 is the Bessel function of the first kind and order, J'_1 is its derivative with respect to its argument $k_c \rho'$, and $k_c a/2 = 1.841$ is the first root of J'_1. E_0 is the electric field at the aperture center ($\rho' = 0$). Since Eq. (13) is not linearly polarized, its use in Eq. (3) provides only part of the total radiated far field. This total field is

$$\boldsymbol{E}(r, \theta, \phi) = jkaE_0 J_1(1.841) \frac{e^{-jkr}}{r} \left\{ \hat{\theta} \cos \phi \frac{J_1\left(\frac{k'a}{2}\right)}{\frac{k'a}{2}} - \hat{\phi} \sin \phi \cos \theta \frac{J_1'\left(\frac{k'a}{2}\right)}{1 - \left(\frac{k'a}{3.682}\right)^2} \right\} \tag{14}$$

in which $k' = k \sin \theta$.

In the E and H planes ($\phi = 0$ and $\pi/2$) the cross-polarized fields cancel and the patterns shown in Fig. 14(a) are similar to those of Eqs. (11) and (12), respectively, but with slightly broader beams and lower sidelobes for the same aperture dimensions. As with rectangular waveguides, open-ended circular waveguide apertures are

insufficiently large for Eq. (14) to represent all the radiated fields accurately. In the principal planes ($\phi = 0$, $\pi/2$) it can give a reasonable approximation for the copolarized fields but fails to accurately represent the cross-polarized field patterns in $\phi = \pi/4$. This is evident from a comparison of numerical results from approximate and exact solutions [Collin (4), p. 233].

Pyramidal and Sectoral Horns

Radiation Patterns. A pyramidal horn fed by a rectangular waveguide supporting the TE_{01} mode has an incident electric field in the aperture of Fig. 6(a) which is approximately the mode distribution modified by a quadratic phase variation in the two aperture dimensions; that is,

$$E_x(x, y, 0) = E_0 \cos\left(\frac{\pi y}{a}\right) \exp\left[-jk\left(\frac{x^2}{2\ell_E} + \frac{y^2}{2\ell_H}\right)\right] \tag{15}$$

With Eq. (15), Eq. (3) becomes

$$\boldsymbol{E}(r, \theta, \phi) = \boldsymbol{A}(r, \theta, \phi) E_0 I_1(k_1) I_2(k_2) \tag{16}$$

where Eq. (5) is used for $\boldsymbol{A}(r, \theta, \phi)$ and

$$I_1(k_1) = \int_{-b/2}^{b/2} \exp\left[-j\left(\frac{\pi x^2}{\lambda \ell_E} - k_1 x\right)\right] dx \tag{17}$$

$$I_2(k_2) = \int_{-a/2}^{a/2} \cos\left(\frac{\pi y}{a}\right) \exp\left[-j\left(\frac{\pi y^2}{\lambda \ell_H} - k_2 y\right)\right] dy \tag{18}$$

The E-plane ($\phi = 0$) and H-plane ($\phi = \pi/2$) radiation patterns are, respectively,

$$\frac{E_\theta(r, \theta)}{E_\theta(r, 0)} = \frac{1 + \cos\theta}{2} \frac{I_1(k \sin\theta)}{I_1(0)} \tag{19}$$

$$\frac{E_\theta(r, \theta)}{E_\theta(r, 0)} = \frac{1 + \cos\theta}{2} \frac{I_2(k \sin\theta)}{I_2(0)} \tag{20}$$

These integrals can be reduced to the Fresnel integrals

$$C(u) - jS(u) = \int_0^u e^{-j(\pi/2)t^2} dt \tag{21}$$

which are tabulated and for which computer subroutines are available. For example,

$$\frac{I_1(k\sin\theta)}{I_1(0)} = e^{j(\pi\ell_E/\lambda)\sin^2\theta}\frac{C(u_2)-C(u_1)-j[S(u_2)-S(u_1)]}{2[C(u)-jS(u)]} \tag{22}$$

with

$$u = \frac{b}{\sqrt{2\lambda\ell_E}} \tag{23}$$

$$\begin{matrix} u_2 \\ u_1 \end{matrix} = \pm u - \sqrt{\frac{2\ell_E}{\lambda}}\sin\theta \tag{24}$$

Figure 3(a) shows plots of the magnitude of Eq. (22) for various values of the E-plane flare parameter $s = b^2/8\lambda\ell_E$, while Fig. 3(b) shows corresponding plots of $|I_2(k\sin\theta)/I_2(0)|$ for the H-plane flare parameter $s = a^2/8\lambda\ell_H$. For no flare ($s = 0$) the patterns are those of a large open-ended rectangular waveguide supporting only the TE_{01} mode. The effect of the flare is to broaden the main beam, raise the sidelobes, and fill pattern nulls. For larger values of s there is enhanced pattern beam broadening and eventually a splitting of the main beam on its axis.

These curves also represent the radiation patterns of the E- and H-plane sectoral horns of Figs. 1(b) and 1(c). For an E-plane sectoral horn ($\ell_H \to \infty$) the E-plane pattern is given by Eq. (19) and the H-plane pattern is given approximately by Eq. (12). For an H-plane sectoral horn ($\ell_E \to \infty$) the E-plane pattern is given approximately by Eq. (11) and the H-plane pattern is given by Eq. (20).

In comparing Figs. 3(a) and 3(b) it is evident that E-plane beamwidths of a square aperture are narrower than H-plane beamwidths. For horns of moderate flare angle and optimum horns the E-plane half-power beamwidth is $0.89\,\lambda/b$ radians and the H-plane half-power beamwidth $1.22\,\lambda/a$ radians. E-plane patterns have minimum sidelobes of -13.3 dB below peak power while H-plane pattern minimum sidelobes levels are -23.1 dB.

The universal patterns of Figs. 3(a) and (b) can also be used to predict the approximate near-field radiation patterns of horns by including the quadratic phase error which is a first-order effect of finite range r. This is done by including

$$e^{-j(\pi/r\lambda)(x^2+y^2)} \tag{25}$$

in Eq. (15). Then the near-field principal plane patterns of a pyramidal horn are given by Eqs. (17) and (18) with ℓ_E, ℓ_H replaced by

$$\ell_E' = \frac{r\ell_E}{r+\ell_E} \tag{26}$$

and

$$\ell_H' = \frac{r\ell_H}{r+\ell_H} \tag{27}$$

These near-field effects are analogous to decreasing the flare length of a horn with a fixed aperture width. The main beam broadens, nulls are filled in, and sidelobes rise.

Limitations and Extensions. Results from Eq. (16) do not apply to small horns and are limited to the forward direction ($\theta < 90^\circ$). They are most accurate on and around the beam axis ($\theta = 0$), becoming progressively less accurate as θ increases. The simplest method for extending the analysis is by the uniform geometrical theory of diffraction [e.g., Love (3), p. 66], which provides the edge-diffracted fields in the lateral and rear directions which receive no direct illumination from the aperture. Only the edges normal to the plane of the pattern contribute significantly to the E-plane pattern but the rear H-plane pattern requires contributions from all four aperture edges and so is difficult to calculate this way.

While the geometry of the pyramidal horn defies rigorous analysis, numerical methods have been used with some success for open waveguides and small horns. For larger horns, this approach becomes computationally intensive, but some results from Liu et al. (5) are shown in Fig. 7 and compared with measurements and approximate computations. Their numerical computations, along with measurements of the aperture fields by Nye and Liang (6) show that higher-order modes need to be added to the dominant mode field of Eq. (15) and that the parabolic phase approximation of Eq. (1) improves as the aperture size increases.

Gain. Pyramidal horns are used as gain standards at microwave frequencies because they can be accurately constructed and their axial directive gain reliably predicted from a relatively simple formula. The ratio of axial far-field power density to the average radiated power density from Eq. (16) yields

$$G = G_0 R_E(u) R_H(v, w) \tag{28}$$

where $G_0 = 32\,ab/(\pi\lambda^2)$ is the gain of an in-phase uniform and cosinusoidal aperture distribution. The reduction of this gain due to the phase variation introduced by the E-plane flare of the horn is

$$R_E(u) = \frac{C^2(u) + S^2(u)}{u^2} \tag{29}$$

where the Fresnel integrals and their argument are defined by Eqs. (21) and (23). Similarly the gain reduction factor due to the H-plane flare of the horn is

$$R_H(v, w) = \frac{\pi^2}{4} \frac{[C(v) - C(w)]^2 + [S(v) - S(w)]^2}{(v - w)^2} \tag{30}$$

where

$$\begin{matrix} v \\ w \end{matrix} = \pm \frac{a}{\sqrt{2\lambda\ell_H}} + \frac{1}{a}\sqrt{\frac{\lambda\ell_H}{2}} \tag{31}$$

A plot of R_E and R_H in decibels as a function of the parameter $2d^2/\lambda\ell$, where d is the appropriate aperture dimension b or a and ℓ is the slant length ℓ_E or ℓ_H, respectively, is shown in Fig. 8. Calculation of the gain from Eq. (28) is accurate to about ± 0.1 dB for 22 dB standard gain pyramidal horns—that is, optimum horns with dimensions of at least 5λ. For 18 dB gain horns the accuracy is about ± 0.2 dB and for 15 dB horns ± 0.5 dB. Since optimum gain pyramidal horns have an aperture efficiency of approximately 50%, the gain is approximately

$$G = 0.5 \frac{4\pi}{\lambda^2} ab \tag{32}$$

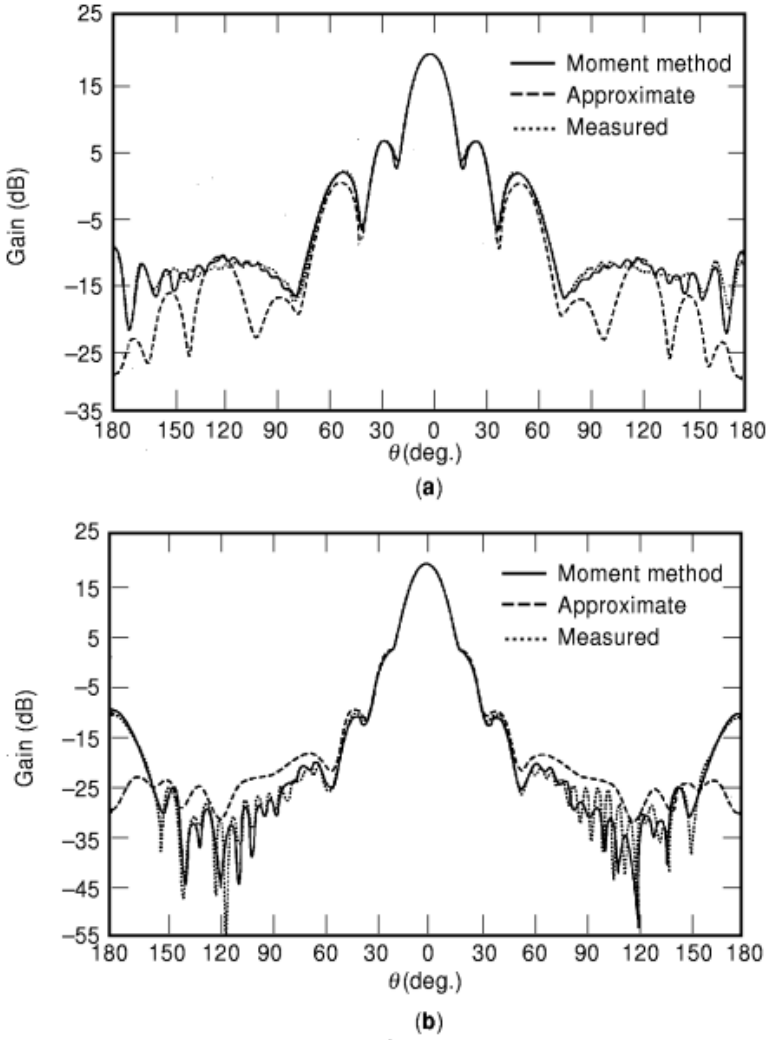

Fig. 7. Calculated and measured (a) E-plane and (b) H-plane radiation patterns of a pyramidal horn of dimensions $a = 4.12\lambda$, $b = 3.06\lambda$, $\ell_E = 10.52\lambda$, and $\ell_H = 9.70\lambda$ [© 1993 IEEE, from Liu et al. (6)].

For an E-plane sectoral horn $\ell_H \to \infty$ and $R_H(v, w) \to 1$ the axial gain is then $G_E = G_0 R_E(u)$, an inaccurate formula because aperture dimension a is less than a wavelength. A result which includes the fact that aperture electric and magnetic fields are not related by free-space conditions and that interaction occurs across the narrow aperture of the horn is

$$G_E = \frac{16ab}{\lambda^2(1+\lambda_g/\lambda)} R_E(u') \exp\left[\frac{\pi a}{\lambda}\left(1 - \frac{\lambda}{\lambda_g}\right)\right] \qquad (33)$$

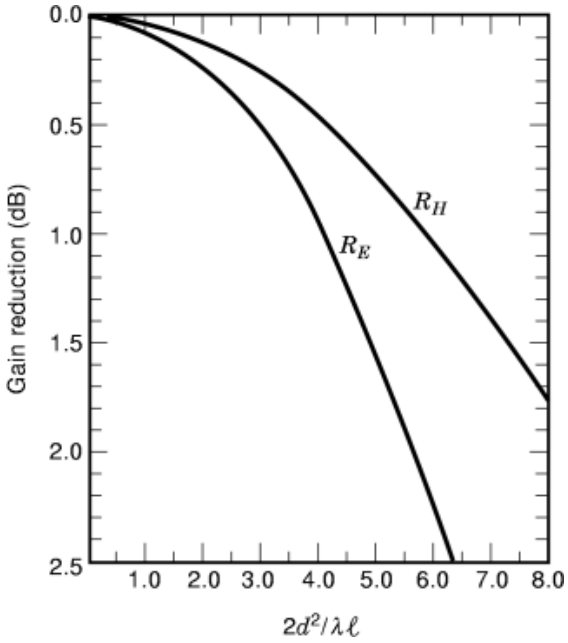

Fig. 8. E- and H-plane flare and near field gain reduction factors R_E and R_H of pyramidal and sectoral horns in decibels [© 1981 IEE, from Jull (11)].

where

$$u' = \frac{b}{\sqrt{2\lambda_g \ell_E}} \tag{34}$$

and

$$\lambda_g = \frac{\lambda}{\sqrt{1-(\lambda/2a)^2}} \tag{35}$$

is the guide wavelength. The accuracy of Eq. (33) is comparable to that of Eq. (28) for the horns of similar b dimension.

The gain of an H-plane sectoral horn, obtained by letting $\ell_E \to \infty$ so that $R_E(u) \to 1$, is $G_H = G_0 R_H(v, w)$. It probably is reasonably accurate, but there appears to be no experimental evidence available to verify it.

The near-field gain of pyramidal and sectoral horns can be calculated from the above expressions by replacing ℓ_E and ℓ_H by Eqs. (26) and (27), respectively.

Conical Horns

The aperture field of a conical horn fed by a circular waveguide supporting the TE_{11} mode is approximately

$$E(\rho', \phi') \exp(-jk\rho'^2/2\ell) \tag{36}$$

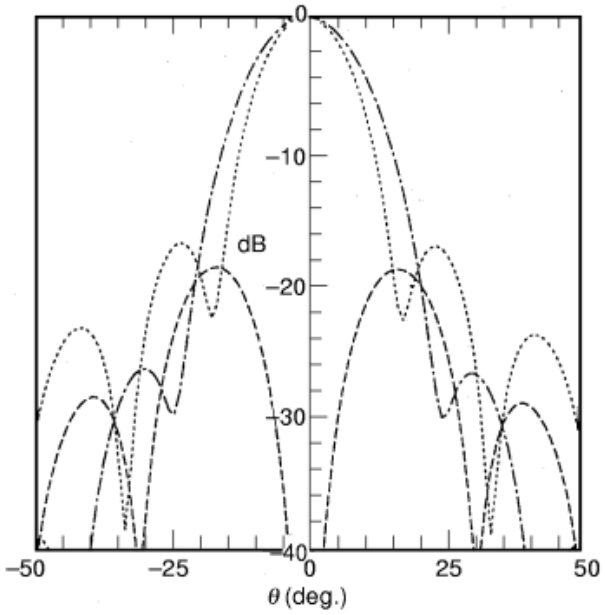

Fig. 9. Copolar and cross-polar radiation patterns for a conical horn with dimensions $a = 4\lambda$ and $\ell = 23\lambda$. — E plane, — H plane, —— cross-polarization [© 1994 IEE, from Olver et al. (7)].

where $\boldsymbol{E}(\rho', \phi')$ is given by Eq. (13) and ℓ is the slant length of the horn. Numerical calculation of the radiation patterns is necessary. In the example of Fig. 9 [Olver et al. (7)] with a flare angle $\alpha = 5^\circ$ and aperture width $a = 4\lambda$, the E-plane ($\phi = 0$) pattern is narrower than the H-plane ($\phi = \pi/2$) pattern as in square rectangular horns. The cross-polar ($\phi = \pi/4$) radiation pattern peak level is -18.7 dB relative to the copolar pattern peak levels, a level typical of conical horn apertures larger than about 2λ. Smaller conical horns can have more axisymmetric patterns. E- and H-plane patterns have equal beamwidths for an aperture diameter $a = 0.96\lambda$, and cross-polarized fields cancel for $a = 1.15\lambda$. This makes small conical horns efficient as reflector feeds and as array elements with high polarization purity.

Larger conical horns are similar to rectangular horns in their lack of axial pattern symmetry. Optimum gain conical horns have an aperture efficiency of about 54% and half-power beamwidths in the E and H planes of $1.05\lambda/a$ and $1.22\lambda/a$ radians, respectively, for aperture diameters of more than a few wavelengths.

Multimode and Corrugated Horns

Lack of axisymmetric radiation patterns make rectangular and conical horns inefficient reflector feeds. Conical horns also have high cross-polarization levels, which are undesirable in a reflector feed. Multimode and corrugated horns were developed largely to overcome these deficiencies. In a dual-mode horn in Love (3, p. 195)

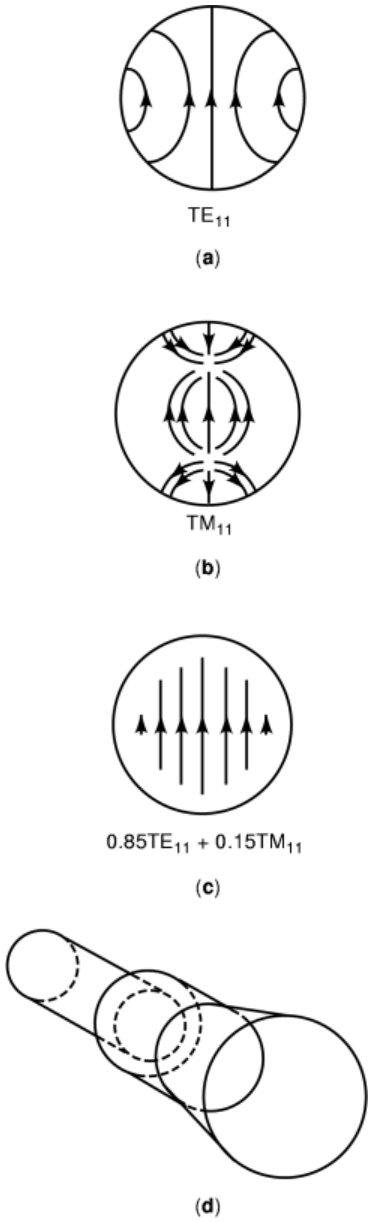

Fig. 10. Excitation of axisymmetric linearly polarized aperture fields in a stepped conical horn [© 1984 McGraw-Hill, Inc. from Love (2)].

this is done by exciting the TM_{11} mode, which propagates for waveguide diameters $a > 1.22\lambda$, in addition to the TE_{11} mode, which propagates for $a > 0.59\lambda$. The electric field configuration of these modes in a waveguide cross section is shown in Figs. 10(a) and (b). Added in phase and in the right proportion, cross-polarized and aperture perimeter fields cancel, while the copolar fields around the aperture centre add, yielding the aperture

field configuration of Fig. 10(c). These mixed mode fields are linearly polarized and tapered approximately cosinusoidally radially across the aperture. This yields the essentially linearly polarized and axisymmetric radiation patterns desired.

Partial conversion of TE_{11} to TM_{11} fields can be effected by a step discontinuity in the circular waveguide feed, as in Fig. 10(d), or by a circular iris or dielectric ring in the horn. The TM_{11}/TE_{11} amplitude ratio depends on the ratio of waveguide diameters, and the relative phase of the modes depends on the length of larger-diameter circular waveguide and the horn. This limits the bandwidth of the horn to about 5%. A multimode square-pyramidal horn has similar low sidelobe level *E*- and *H*-plane radiation patterns due to an essentially cosinusoidal aperture distribution in the *E*-plane as well as the *H*-plane [Love (2)]. This can be achieved by excitation of a hybrid TE_{21}/TM_{21} mode by an *E*-plane step discontinuity or by changes in the *E*-plane flare.

Corrugated horns have aperture fields similar to those of Fig. 10(c) and consequently similar radiation patterns, but without the frequency bandwidth limitations of the above horn. This is achieved by introducing annular corrugations in the interior walls of a conical horn. There must be sufficient corrugations per wavelength (at least three) that the annular electric field E_ϕ is essentially zero on the interior walls. The corrugations make H_ϕ also vanish. This requires corrugation depths such that short circuits at the bottom of the grooves appear as open circuits at the top, suppressing axial current flow on the interior walls of the horn. This groove depth is $\lambda/4$ on a plane corrugated surface or a curved surface of large radius. For a curved surface of smaller radius, such as near the throat of the horn, the slot depths need to be increased; for example, for a surface radius of 2λ, the depth required is 0.3λ. Usually slots are normal to the conical surface in wide flare horns but are often perpendicular to the horn axis with small flares. To provide a gradual transition from the TE_{11} mode in the waveguide to a hybrid HE_{11} mode in the aperture, the depth of the first corrugation in the throat should be about 0.5λ so that the surface there resembles that of a conducting cone interior. Propagation in corrugated conical horns can be accurately calculated numerically by mode-matching techniques. The aperture field is approximately

$$E_x(\rho') = AJ_0(k_c\rho') \exp\left(\frac{-jk\rho'^2}{2\ell}\right) \tag{37}$$

where $k_c a/2$ is 2.405, the first zero of the zero-order Bessel function J_0, ℓ is the slant length of the horn, and A is a constant. This aperture field is similar to that of Fig. 10(c), and the resulting *E* and *H* patterns are similarly equal down to about -25 dB. Some universal patterns are shown in Fig. 11. Cross-polarization fields are also about -30 dB from the axial values, but are now over a bandwidth of 2:1 or more.

Broadband axisymmetric patterns with low cross-polarization make corrugated horns particularly attractive as feeds for reflectors. Low cross-polarization allows the use of dual polarization to double the capacity of the system. Another notable feature for this application is that the position of the *E*- and *H*-plane pattern phase centers coincide. Figure 12 shows the distance of the phase center from the horn apex, divided by the slant length, of small-flare-angle conical [Milligan (8)] and corrugated [Thomas (9)]] horns for values of the phase parameter *s* given by Eq. (2). For a conical horn the *E*-plane phase center is significantly further from the aperture than the *H*-plane phase center. Thus if a conical horn is used to feed a parabolic reflector, the best location for the feed is approximately midway between the *E*- and *H*-plane phase centers. With a corrugated horn, such a compromise is not required so it is inherently more efficient.

Corrugated horns may have wide flare angles, and their aperture size for optimum gain decreases correspondingly. For example, with a semiflare angle of 20° the optimum aperture diameter is about 8λ, whereas for a semiflare angle of 70° it is 2λ. Wide-flare corrugated horns are sometimes called “scalar horns” because of their low cross-polarization levels.

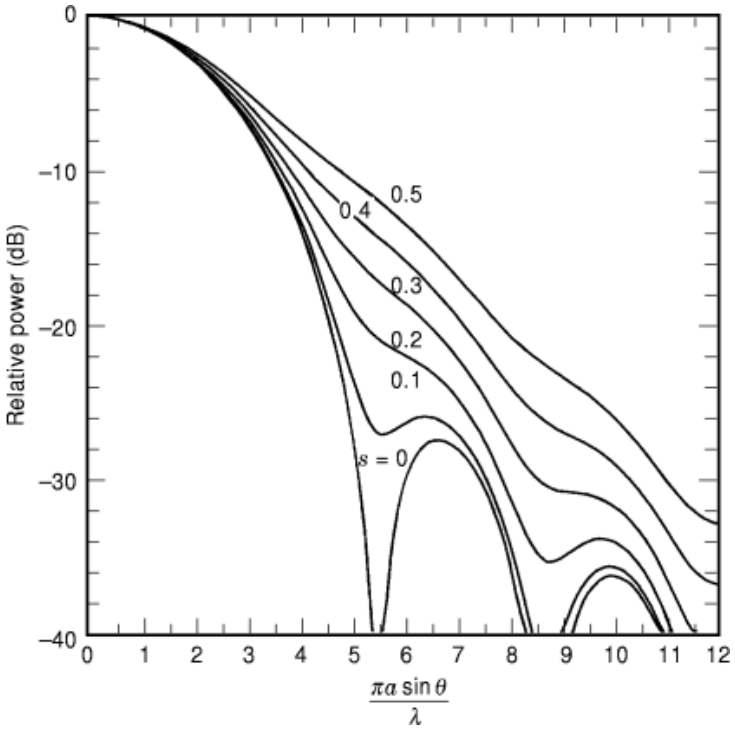

Fig. 11. Universal patterns of small-flare-angle corrugated horns as a function of the parameter $s = a^2/8\lambda\ell$ [© 1984 McGraw-Hill, Inc. from Love (2)].

Profile Horns

Most corrugated horns are conical with a constant flare angle. Figure 13 shows a profile conical horn in which the flare angle varies along its length. This arrangement provides a horn shorter than a conical corrugated horn of similar beamwidth, with a better impedance match due to the curved profile at the throat and an essentially in-phase aperture field distribution due to the profile at the aperture. Consequently the aperture efficiency is higher than that of conical corrugated horns. The phase center of the horn is near the aperture center and remains nearly fixed over a wide frequency band. Radiation patterns of a profile horn similar to that of Fig. 13 are shown in Fig. 14 [Gonzalo et al. (10)]. The patterns are similar to those of a Gaussian beam, such as is radiated from the end of an optical fiber supporting the HE_{11} mode. The performance of this small horn as a feed seems close to ideal, but larger profile horns may exhibit higher sidelobe levels due to excitation of the HE_{12} mode at the aperture.

Horn Impedance

Antennas must be well matched to their transmission lines to ensure a low level of reflection in microwave communication systems. The impedance behavior of a horn depends on the mismatch at the waveguide/horn junction and at its aperture. For an *E*-plane sectoral horn, reflections from these discontinuities are comparable in magnitude; and since they interfere, the total reflection coefficient oscillates with frequency and the input voltage standing wave ratio (*VSWR*) may vary from 1.05 at high frequencies to 1.5 at the lowest frequency. With

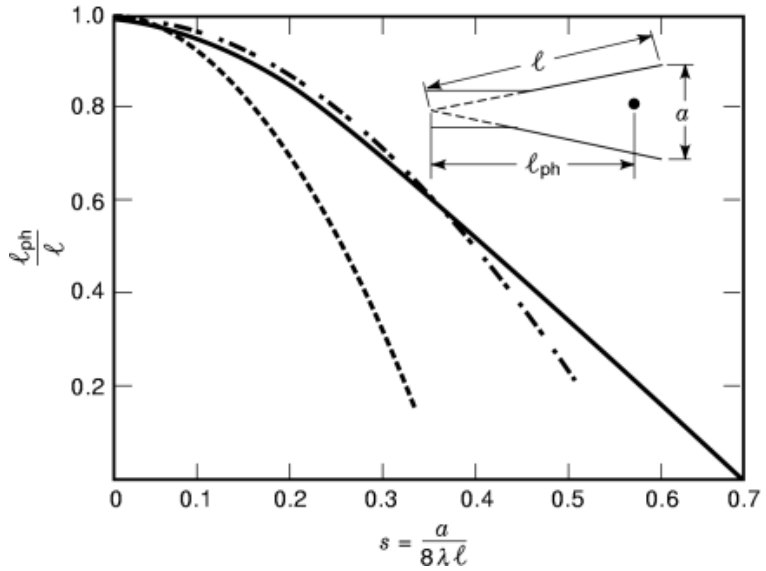

Fig. 12. Normalized distance of the phase center from the apex of conical (— *E* plane, — *H* plane) and corrugated (———) horns [Data from Milligan (8) and Thomas (9)].

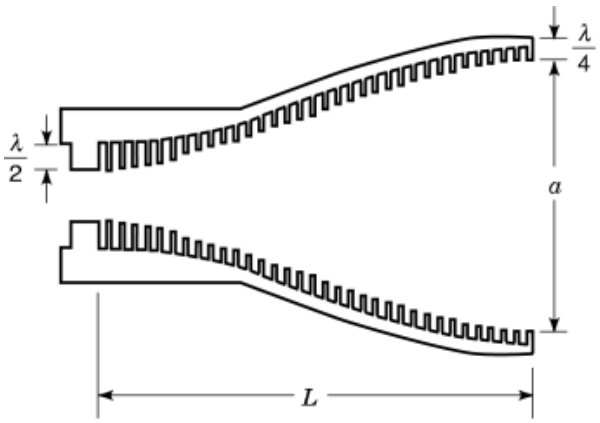

Fig. 13. A profile corrugated horn [© 1994, IEE, from Olver et al. (7)].

H-plane sectoral horns, aperture reflection is much stronger than junction reflection so their VSWR increases almost monotonically with decreasing frequency. An inductive iris in the waveguide near the *E*-plane horn junction can match its discontinuity. A capacitive iris may be similarly used for an *H*-plane sectoral horn. Aperture reflections in these horns may be matched with dielectric covers.

Pyramidal horns of sufficient size and optimum design tend to be inherently well-matched to their waveguide feeds because the *E*- and *H*-plane aperture and flare discontinuities partially cancel. For example, a 22 dB gain horn has a VSWR of about 1.04 while an 18 dB horn has a VSWR of less than 1.1.

Conical horns fed by circular waveguides supporting the dominant TE_{11} mode have an impedance behavior similar to that of pyramidal horns of comparable size fed by rectangular waveguides. The waveguide/horn discontinuities of both horns may be matched by an iris placed in the waveguide near the junction. A broader

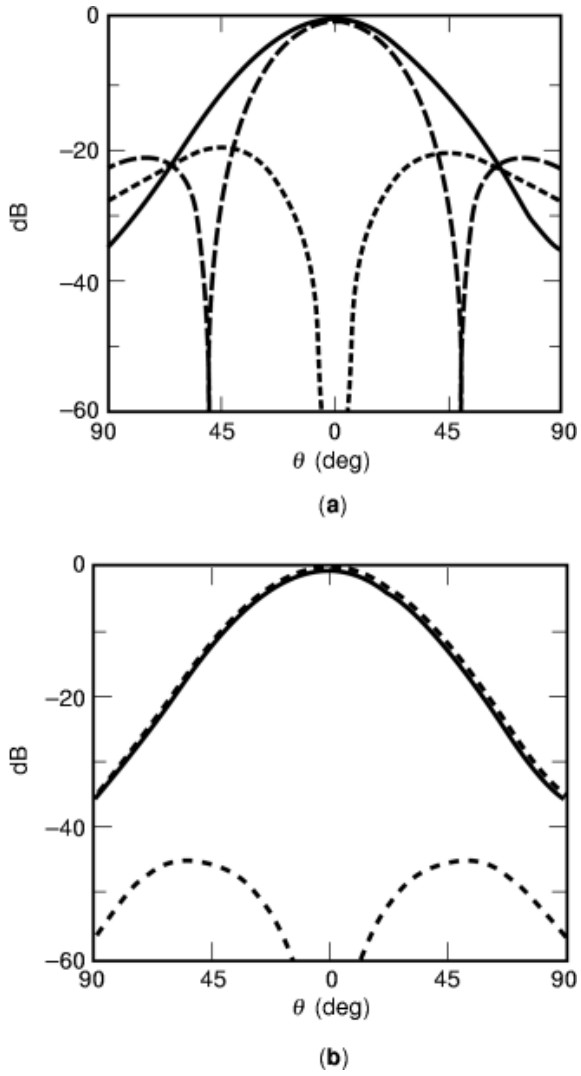

Fig. 14. (a) Far-field radiation patterns of TE_{11} mode and (b) radiation patterns of a profile corrugated horn of aperture $a = 15.8$ mm and length $L = 26.7$ mm at 30 GHz. − − −E plane,———H plane ··· cross-polarization [© 1997, IEEE, from Gonzalo et al. (10)].

bandwidth match is provided by a curved transition between the interior walls of the waveguide and the horn. Broadband reduction of aperture reflection may be similarly reduced by a curved surface of a few wavelengths radius. Such "aperture-matched" horns also have lower sidelobe levels and less back radiation in their E-plane patterns than do conventional pyramidal and conical horns. Their H-plane flare patterns are affected little by such aperture matching because the electric field vanishes at the relevant edges.

For dual-mode and corrugated horns there are also negligible fields at the aperture edges and hence little diffraction there. Corrugated horns with initial groove depths near the throat of about a half-wavelength and which gradually decrease to a quarter-wavelength near the aperture, as in Fig. 13, are well-matched at both throat and aperture. For most well-designed corrugated horns a VSWR of less than 1.25 is possible over a

frequency range of about 1.5:1. Dual-mode horns using a step discontinuity as in Fig. 10(d) may have a VSWR of 1.2 to 1.4. If an iris is required for a match, the frequency bandwidth will of course be limited. Conical and pyramidal horns using flare-angle changes to generate the higher-order modes can have VSWRs less than 1.03 and require no matching devices.

BIBLIOGRAPHY

1. J. F. Ramsay, Microwave antenna and waveguide techniques before 1900, *Proc. IRE*, **46**: 405–415, 1958.
2. A. W. Love, Horn antennas, in R. C. Johnson and H. Jasik (eds.), *Antenna Engineering Handbook*, 2nd ed., New York: McGraw-Hill, 1984, chap. 15.
3. A. W. Love (ed.), *Electromagnetic Horn Antennas*, Piscataway, NJ: IEEE Press, 1976.
4. R. E. Collin, *Antennas and Radiowave Propagation*, New York: McGraw-Hill, 1985.
5. K. Liu *et al.*, Analysis of pyramidal horn antennas using moment methods, *IEEE Trans. Antennas Propag.*, **41**: 1379–1389, 1993.
6. J. F. Nye, W. Liang, Theory and measurement of the field of a pyramidal horn, *IEEE Trans. Antennas Propag.*, **44**: 1488–1498, 1996.
7. A. D. Olver *et al.*, *Microwave Horns and Feeds*, vol. 39, London: IEE Electromagnetic Waves Series, 1994.
8. T. Milligan, *Modern Antenna Design*, New York: McGraw-Hill, 1985, chap. 7.
9. B. M. Thomas, Design of corrugated horns, *IEEE Trans. Antennas Propag.*, **26**: 367–372, 1978.
10. R. Gonzalo, J. Teniente, C. del Rio, Very short and efficient feeder design from monomode waveguide, *IEEE Antennas Propag. Soc. Int. Symp. Dig.*, Montreal, 1997, pp. 468–470.
11. E. V. Jull, *Aperture Antennas and Diffraction Theory*, vol. 10, London: IEE Electromagnetic Waves Series, 1981.

EDWARD V. JULL
University of British Columbia